

CCA-1792

YU ISSN 0011-1643

UDC 543.42

Author's Review

Vibrational Spectroscopy and Structural Phase Transitions in Molecular Crystals

A. Novak

Laboratoire de Spectrochimie Infrarouge et Raman, CNRS, 2 rue Henri Dunant,
94320 Thiais, France

Received March 23, 1987

Vibrational spectroscopy can give useful information, both structural and dynamical, about phase transitions in molecular crystals. In particular, the data concerning the mechanism of the transformation at molecular level can be obtained. This is illustrated by examples of pure van der Waals crystals such as 3,5-dichloropyridine and 4-methylpyridine, hydrogen bonded malonic acid, inorganic ferroelectrics cesium dihydrogen phosphate and triammonium hydrogen disulphate, a superionic protonic conductor cesium hydrogen sulphate and a coordination compound: propylene diammonium manganese tetrachloride.

INTRODUCTION

Vibrational spectroscopy has been widely used in the study of structural phase transitions of a number of crystals¹⁻⁸ and can give useful information about phases and their transformation, *i. e.* about the structural and dynamic aspects, respectively. As far as crystalline structures are concerned, X-ray and/or neutron diffraction methods and vibrational spectroscopy are complementary. The latter is particularly useful in determining the position of the proton in strong hydrogen bonds, the symmetry of disordered crystals and the nature and degree of disorder, for example. If there are no X-ray data, which frequently happens for low temperature phases, the vibrational spectroscopy may help to find out the space group and the number of molecules in the unit cell. It can also identify non-equivalent molecules and in the case of hydrogen bonded crystals the type of molecular association. The spectroscopic data are used in studying the dynamics of phase transitions and this area was developed particularly fast after the theoretical investigations of Cochran⁹ who worked out the dynamical concept of phase transitions implying soft mode and are helpful in determining the order—first or second—of the transformation, whether its nature is of displacive order-disorder (or mixed) or reconstructive type and the mechanism at the molecular level. Such information can be obtained by studying the frequency, intensity and half-width of infrared and Raman bands as a function of temperature and pressure. The low-frequency bands associated with lattice modes generally appear more phase transition sensitive than high-frequency bands due to intramolecular vibrations.

We were interested in the relationship which may exist between the mechanism of a given phase transition and the nature of intermolecular forces responsible for the cohesion of the crystal. We have thus examined a number of different types of compounds: (a) pure van der Waals crystals such as tetrahalobenzenes¹⁰, pyrazine¹¹, 3,5-dichloropyridine¹², γ -picoline¹³ and malononitrile^{14,15}, (b) hydrogen-bonded organic crystals like oxalic¹⁶, malonic¹⁷ and squaric¹⁸ acid, (c) inorganic ferroelectrics cesium dihydrogen phosphate CsH_2PO_4 ¹⁹, rubidium dideuterium phosphate RbD_2PO_4 ²⁰, triammonium hydrogen disulphate $(\text{NH}_4)_3\text{H}(\text{SO}_4)_2$ ²¹, (d) superionic protonic conductors, hydrated uranyl phosphate (HUP) $\text{H}_3\text{O}^+\text{UO}_2\text{PO}_4 \cdot 3\text{H}_2\text{O}$ ²², cesium hydrogen sulphate CsHSO_4 ²³ and selenate CsHSeO_4 ²⁴, (e) organometallic and coordination compounds such as $\text{MgBr}_2 \cdot 2(\text{C}_2\text{H}_5)_2\text{O}$ ²⁵, propylene diammonium manganese tetrachloride $(\text{NH}_3(\text{CH}_2)_3\text{NH}_3)\text{MnCl}_4$ ^{26,27}, ferrocene and nickelocene²⁸.

In this paper, we are reviewing some recent examples of various types of crystals investigated in our laboratory in order to show typical structural and dynamical information that vibrational spectroscopy can give about different phase transitions in molecular crystals.

1. 3,5-DICHLOROPYRIDINE, $\text{C}_5\text{H}_3\text{NCl}_2$

3,5-Dichloropyridine (DCP) (Figure 1) undergoes two phase transitions at 287.5 and 167.5 K with the corresponding enthalpies of 1200 and 0.4 J mole⁻¹, respectively, as shown by calorimetric measurements.¹² There are thus three crystalline phases: *I* above 287.5 K, *II* between 287.5 and 167.5 K and *III* below 167.5 K. The *I*↔*II* transition has been confirmed by nuclear quadrupole resonance of both ³⁵Cl and ¹⁴N nuclei. The *II*—*III* transition is difficult to determine with accuracy by ³⁵Cl NQR while ¹⁴N NQR does not give any indication of this transition.

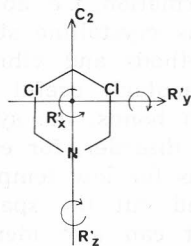


Figure 1. Molecule of 3,5-dichloropyridine; R'_x , R'_y and R'_z : librational motions about the axes of the smallest, intermediate and largest moment of inertia, respectively; C_2 -binary axis.

Infrared and Raman spectra of DCP have been recorded at various temperatures between 15 and 300 K in the regions of both intramolecular and lattice vibrations.¹² The latter are much more temperature sensitive than the former and are shown in Figures 2 and 3. General pattern of both Raman and infrared spectra is different for the three phases, the largest change being observed for the *I*↔*II* phase transition. The temperature dependence of frequencies and Raman intensities of lattice bands shows clearly the *II*↔*III* phase transition in the 150—170 K region (Figure 4).

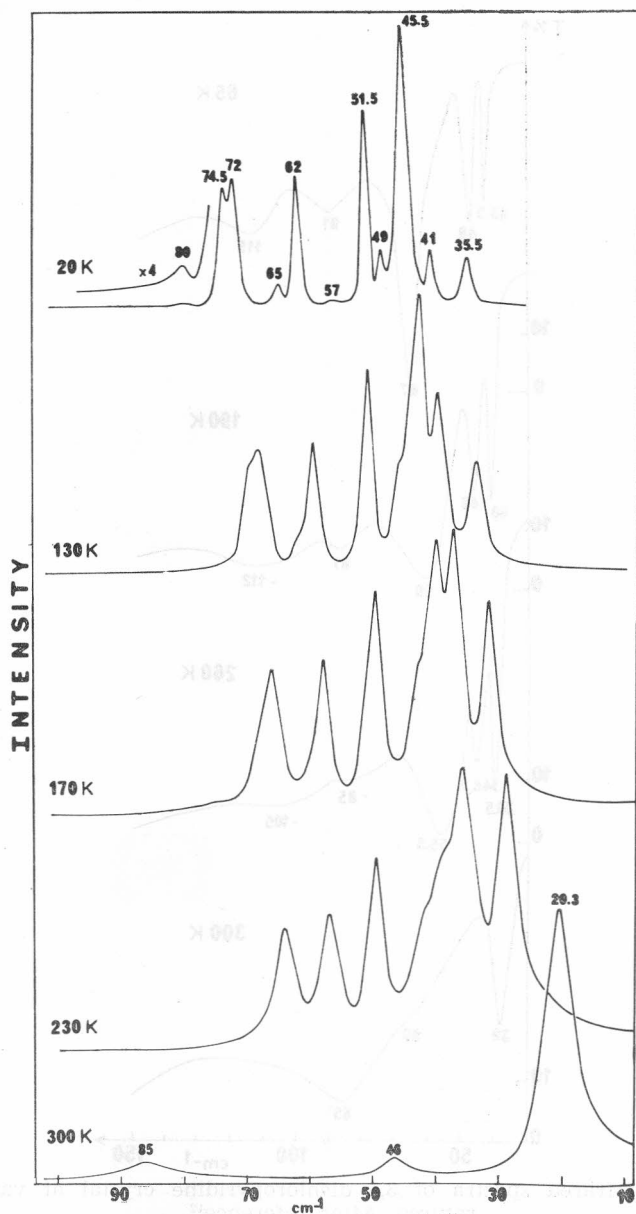


Figure 2. Low-frequency Raman spectra of 3,5 dichloropyridine crystal at various temperatures. After reference¹².

Crystalline Structures

Phase I of DCP has been investigated by X-ray diffraction: the crystal belongs to the monoclinic system with the space group either $P2_1/m$ or $P2_1$ and $Z = 2$. The NQR of ^{35}Cl shows only one frequency, implying that all Cl atoms are equivalent: the site symmetry of DCP molecules is thus C_2

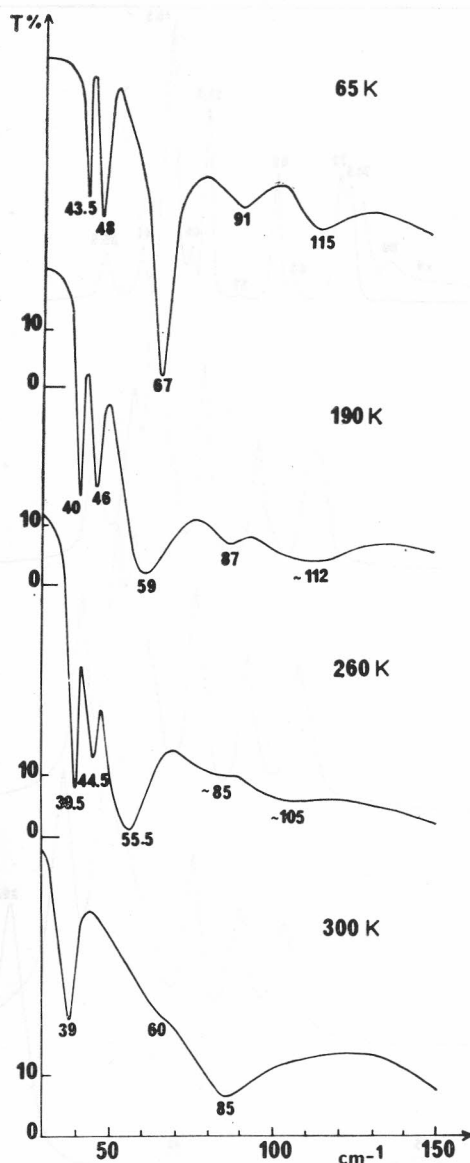


Figure 3. Far-infrared spectra of 3,5 dichloropyridine crystal at various temperatures. After reference¹².

or C_s . The vibrational spectra indicate the existence of symmetry centers since several internal frequencies show a significant g-u splitting and help to choose the $P2_1/m$ space group. The corresponding factor group analysis predicts nine external modes represented by: $3A_g(R'y, 2T') + 3B_g(R'x, R'z, T') + 2A_u(R'x, R'z) + 1B_u(R'y)$ where R' and T' are rotational and translational vibrations. Librations designated by R'x correspond to rotational motions about the x-axis perpendicular to the molecular plane, R'z about

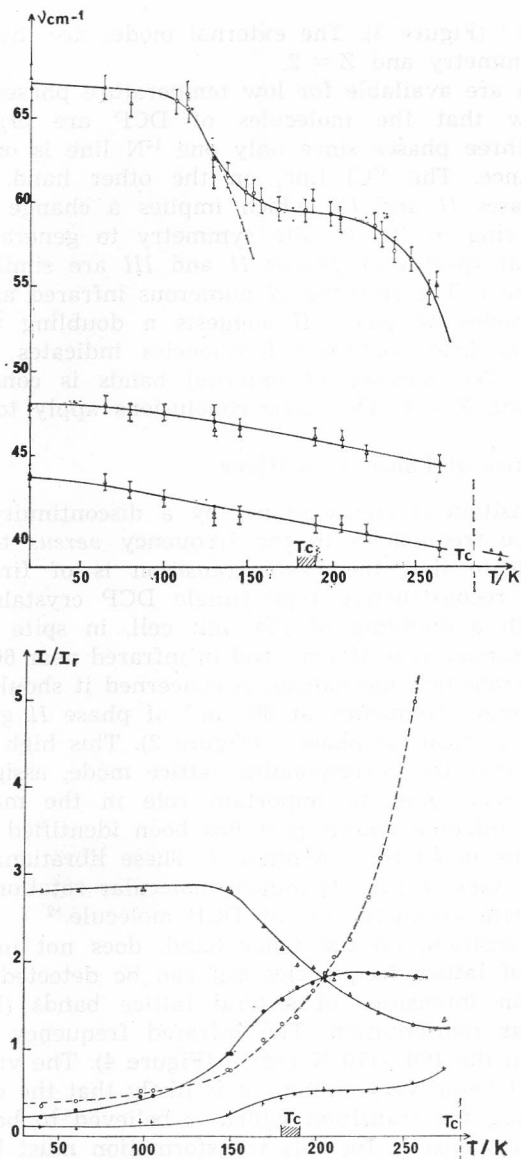


Figure 4. Temperature dependence of far-infrared frequencies (above) and Raman intensities (below) of some lattice bands of 3,5 dichloropyridine crystal. After reference¹².

z-axis which coincides with the two-fold molecular axis (C_2) and $R'y$ about the y-axis perpendicular to the the x and z axes (Figure 1). Different geometries of Raman scattering on a single crystal of DCP helped to assign five lattice fundamentals out of the six expected: $3A_g$ at $34(T')$, $46(T')$ and $85(R'y)$ cm^{-1} and $2B_g$ at $20.5(R'x, R'z)$ and $46(R'z, R'x)$ cm^{-1} (Figure 2). All the three infrared bands were identified at $39(Au, R'x, R'z)$, $60(Au, R'x, R'z)$

and $85(\text{Bu}, \text{R}'\gamma) \text{ cm}^{-1}$ (Figure 3). The external modes are thus also consistent with the $P2_1/m$ symmetry and $Z = 2$.

No X-ray data are available for low temperature phases *II* and *III*. The NQR results show that the molecules of DCP are crystallographically equivalent in all three phases since only one ^{14}N line is observed for each ν_+ and ν_- resonance. The ^{35}Cl line, on the other hand, splits into two components in phases *II* and *III* which implies a change of crystal symmetry and a lowering of the C_s site symmetry to general position below 275 K.¹² Vibrational spectra of phases *II* and *III* are similar but different from those of phase *I*. The splitting of numerous infrared and Raman bands due to internal modes of phase *II* suggests a doubling of the unit cell while the non-coincidence of their frequencies indicates the presence of symmetry centers. The number of external bands is consistent with the C_{2h} factor group and $Z = 4$. The same conclusions apply to phase *III*.

Nature and Dynamics of Phase Transitions

The $I \leftrightarrow II$ transition is characterized by a discontinuity of the Raman and infrared lattice frequencies in the frequency *versus* temperature plot. These results indicate that the $I \leftrightarrow II$ transition is of first order and is likely to be of a reconstructive type (single DCP crystals shatter during the transition) with a doubling of the unit cell, in spite of two strongly damped modes in Raman near 30 cm^{-1} and in infrared near 60 cm^{-1} (Figure 4).

As far as the transition mechanism is concerned it should be pointed out that the lowest Raman frequency at 30 cm^{-1} of phase *II* goes over to that at 20 cm^{-1} in the spectrum of phase *I* (Figure 2). This high phase transition sensitivity implies that the corresponding lattice mode, assigned to a mixed $\text{R}'x, \text{R}'z$ libration must play an important role in the mechanism of the transformation. Its infrared counterpart has been identified near 60 cm^{-1} in phase *II* and softens to 39 cm^{-1} in phase *I*. These librational motions about x and z molecular axes (Figure 1) induce molecular rotation which destroys or creates the C_s site symmetry of the DCP molecule.¹²

The $II \leftrightarrow III$ transition, on the other hand, does not manifest itself by any discontinuity of lattice frequencies but can be detected from a relative variation of Raman intensities of several lattice bands (Figure 4) which implies a molecular reorientation. The infrared frequency at 67 cm^{-1} also sharply decreases in the 100—170 K region (Figure 4). The vibrational spectra of phases *II* and *III* being very similar, it is likely that the crystal symmetry is not broken during the transition which is believed to be of a displacive type. The motion responsible for this transformation must be sought in the behaviour of the 67 cm^{-1} infrared frequency which drops to 59 cm^{-1} in phase *II*: it corresponds to a predominantly $\text{R}'z$ libration, *i. e.* a rotation about the C_2 molecular axis since there is no anomaly in the ^{14}N NQR spectra at this temperature.¹²

2. 4-METHYLPYRIDINE (γ -PICOLINE), $\text{CH}_3\text{-C}_5\text{H}_4\text{N}$

4-methylpyridine (4MP) crystal is interesting since, besides the low frequency lattice modes, the rotational — or torsional motion of methyl group plays an important role in the mechanism of phase transitions.¹³ The first transition at 254 K has been evidenced by calorimetry and ^{14}N nuclear

quadrupole resonance.²⁹ The results of the vibrational spectroscopy, *i. e.* band splitting and slope discontinuities in the Raman lattice frequencies *versus* temperature plot as well as internal band splitting, confirm this transition and show a new one at 100 K. There are thus three different phases in 4MP between 5 K and the melting point 276.8 K: phase I (254—276.8 K), phase II (100—254 K) and phase III (5—100 K).

Symmetry and structure

Phase II

The only crystalline structure which has been determined by X-ray diffraction is that of phase II (Figure 5).³⁰ At 120 K, 4MP crystal is tetragonal $I4_1/a$ (C_{4h}^6) with four molecules in the primitive unit cell and the C_2 site symmetry implying a disordered methyl group. The corresponding factor group analysis predicts twelve lattice modes, eight Raman ($2A_g + 2B_g + 4E_g$) and four infrared ($A_u + 3E_u$) active. Three infrared absorption bands have been observed at 98, 63 and 38 cm^{-1} and assigned to mixed R' and T' motions. Five Raman bands at 108, 83, 74, 67.5 and 59 cm^{-1} are

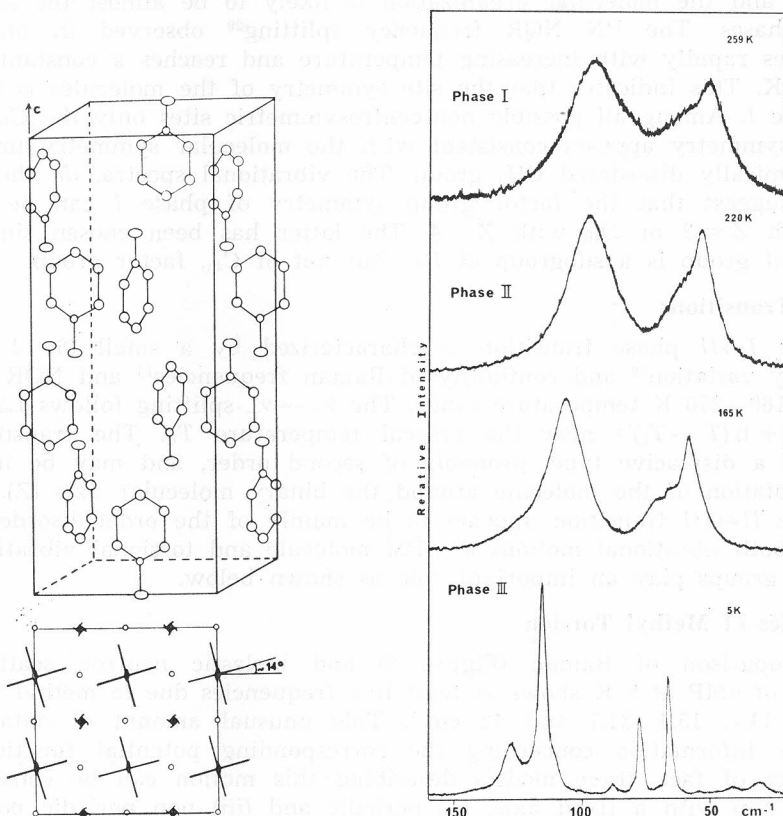


Figure 5. (left) Crystal structure of γ -picoline in phase II. After reference³⁰.
Figure 6. (right) Low-frequency Raman spectra of 4-ethylpyridine crystal at various temperatures (a) phase I, (b) phase II, (c) phase III. After reference¹³.

also assigned to mixed rotational-translational modes, except for the 108 cm^{-1} band which is due to a predominant R_z libration, *i.e.* libration about the binary axis¹³ (Figure 6).

Phase III

X-ray powder diffraction data at 93 K suggest a $P2_1/c \equiv C_{2h}^5$ space group with four molecules in the unit cell.³¹ Symmetry lowering is manifested spectroscopically by the splitting of several internal modes which were degenerate (Eg, Eu) in phase II. Ag—Bg splitting gives rise to Raman components of different intensities indicating a C_1 site symmetry of the 4MP molecule since equal intensity of Ag—Bg components is expected for C_s site symmetry. The methyl groups are thus frozen in a non-symmetric conformation with respect to the aromatic molecular plane. Seven infrared and eight Raman external bands out of the nine and twelve, respectively, expected for the C_{2h} symmetry and $Z = 4$, have been observed (Figure 6).

Phase I

The Raman as well as the infrared spectra of phases II and I are rather similar and the molecular organization is likely to be almost the same in both phases. The ^{14}N NQR frequency splitting²⁹ observed in phase II decreases rapidly with increasing temperature and reaches a constant value at 254 K. This indicates that the site symmetry of the molecules is higher, in phase I. Among all possible non-centrosymmetric sites only the C_{2v} point group symmetry appears consistent with the molecular symmetry implying a dynamically disordered CH_3 group. The vibrational spectra, on the other hand, suggest that the factor group symmetry of phase I can be either C_{4h} with $Z = 2$ or D_{4h} with $Z = 4$. The latter has been chosen since the C_{2v} point group is a subgroup of D_{4h} , but not of C_{4h} , factor group.

Phase Transitions

The $I \leftrightarrow II$ phase transition is characterized by a small (60 J mol^{-1}) enthalpy variation²⁹ and continuity of Raman frequencies¹³ and NQR lines²⁹ in the $160\text{--}270\text{ K}$ temperature range. The $\nu_+ - \nu_-$ splitting follows Landau's law: $a + b(T - T_c)^{1/2}$ near the critical temperature T_c . The transition is thus of a displacive type, probably of second order, and may be induced by a rotation of the molecule around the binary molecular axis (Z).

The $II \leftrightarrow III$ transition appears to be mainly of the order-disorder type where both librational motions of 4PM molecule and torsional vibrations of methyl groups play an important role as shown below.

Dynamics of Methyl Torsion

Comparison of Raman (Figure 7) and inelastic neutron scattering³² spectra of 4MP at 5 K shows at least five frequencies due to methyl torsion at 4.2, 11.5, 15.4, 31.7 and 42 cm^{-1} . This unusual amount of data gives accurate information concerning the corresponding potential function. As a matter of fact, three models describing this motion can be considered: (i) free top with a fixed axis, (ii) periodic and (iii) non periodic potential function.

The above frequencies as well as those of the totally deuterated derivative, 4MP- d_7 , do not fit the first two models but are in agreement with

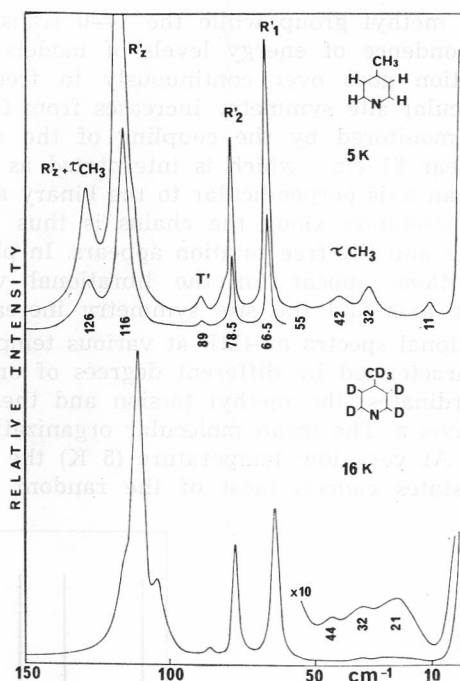


Figure 7. Low-frequency Raman spectra of 4-methylpyridine crystal at liquid helium temperature: (a) 4-methylpyridine- h_7 , (b) 4-methylpyridine- d_7 . After reference¹³.

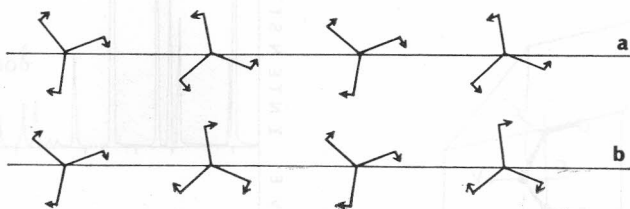


Figure 8. Tentative structure of γ -picoline at 5 K consistent with methyl group torsions correlated along infinite chains: (a) out-of-phase torsion, (b) in-phase torsion. After reference¹³.

the assumption that in the low-temperature phase *III* the torsional motion of CH_3 group loses its periodic character and may be approximated by a Taylor series expansion about the equilibrium position. The non-periodic potential implies that the CH_3 torsion induces some deformation of the crystal which cannot be suppressed after $2\pi/3$, $4\pi/3$ or 2π rotation. This happens if methyl groups are correlated along infinite chains and if their rotations are coupled much in the same way as gear wheels, as shown in Figure 8. The non periodic potential corresponds thus to out-of-phase rotations and reflects the imperfection of methyl-methyl correlation and/or some dephasing along the chains, which prevents the recovery of the initial state after CH_3 rotation.¹³

In phase *II* near 100 K, the Raman τCH_3 bands at 32 and 42 cm^{-1} (at 5 K) converge to 50 cm^{-1} band which has been assigned to the $3 \leftarrow 0$ transition

of a freely rotating methyl group while the $1 \leftarrow 0$ transition is observed at 5 cm^{-1} . The correspondence of energy levels of models (I) and (III) shows that aperiodic function goes over continuously to freely rotating methyl group and the molecular site symmetry increases from C_1 to C_2 . The $III \leftrightarrow II$ phase transition is monitored by the coupling of the methyl torsion with an external mode near 61 cm^{-1} which is interpreted as a mainly rotational vibration R' around an axis perpendicular to the binary axis of the molecule: the methy-methyl correlation along the chains is thus destroyed when the temperature increases and the free rotation appears. In phase I, above 254 K , large amplitude motions appear for the librational vibration about the binary (z) molecular axis and the site symmetry increases to C_{2v} .

Thus, the vibrational spectra of 4MP at various temperatures show three different phases characterized by different degrees of order (disorder) along two vibrational coordinates: the methyl torsion and the molecular libration around the binary axis z . The mean molecular organization is rather similar in all three phases. At very low temperature (5 K) the depopulation of the excited librational states cancels most of the random fluctuations of the

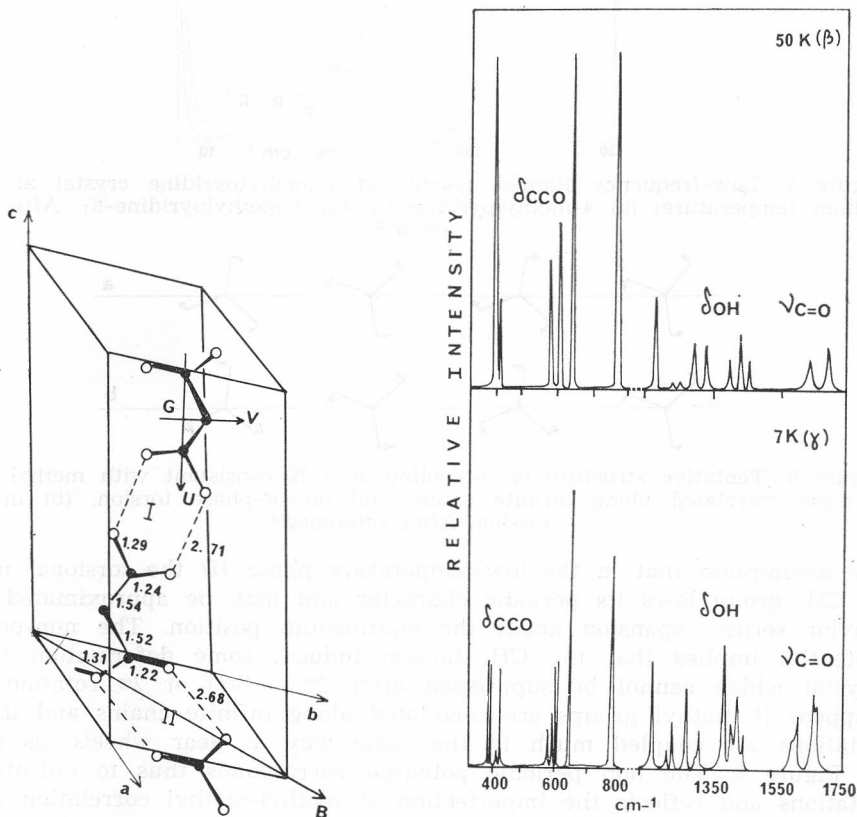


Figure 9. (left) Crystal structure of the room temperature β phase of malonic acid after reference³⁷. B is the direction which becomes the two fold axis in the α phase. Figure 10. (right) High frequency Raman spectra of malonic acid at 50 K (β phase) and 7 K (γ phase). After reference³⁶.

crystal field due to phonons and weak methyl-methyl interactions become dominant providing a new ordered crystalline state with a singular methyl dynamics.¹³

3. MALONIC ACID, $\text{CH}_2(\text{COOH})_2$

Two structural phase transitions at 360 and 48 K have been observed for the malonic acid crystal using calorimetric and spectroscopic measurements.³³⁻³⁶ There are thus three crystalline phases, designated α (above 360 K), β (360–48 K) and γ (below 48 K).

β -Phase

The structure of the β phase alone has been determined by X-ray diffraction³⁷: the crystal is triclinic with the $P\bar{1}$ space group and two molecules per unit cell; the molecules are linked through hydrogen-bonded dimer rings into infinite chains. There are two crystallographically non-equivalent dimer rings, nearly orthogonal to each other, with different C=O, C—O, C—C and O...O distances³⁷ (Figure 9). The existence of centrosymmetric dimers is shown spectroscopically following the mutual exclusion rule, *i.e.* the infrared and Raman frequencies generally do not coincide; in the case of the characteristic $\nu\text{C}=\text{O}$ vibration, for instance, the average infrared frequency at 1765 cm^{-1} is considerably different from the Raman value at 1650 cm^{-1} .³⁸ The presence of non-equivalent dimers, on the other hand, may be sought in the appearance of doublets of the $\nu\text{C}=\text{O}$ mode at $1630\text{--}1670\text{ cm}^{-1}$ in Raman (Figure 10) and at $1690\text{--}1740\text{ cm}^{-1}$ in infrared, as well as of other characteristic bands such as δOH , $\nu\text{C—C}$, δCCO ,... (Figure 10).³⁸

γ -Phase

When the crystal is cooled below 48 K, the corresponding Raman spectra are modified in the region of internal and external vibrations.³⁶ In the high frequency region (Figure 10) doublets of characteristic bands split into quadruplets: for $\nu\text{C}=\text{O}$ mode, for instance, four Raman components at 1622, 1629, 1676 and 1683 cm^{-1} , are observed. The infrared-Raman exclusion, on the other hand, persists. These spectroscopic data indicate a doubling of the unit cell with the symmetry centres preserved. A $P\bar{1}$ space group with the unit cell containing four non-equivalent dimer rings can thus be suggested³⁶, in agreement with the ENDOR study showing four magnetically non equivalent protons of this compound at liquid helium temperature³⁹.

$\beta\leftrightarrow\gamma$ Phase Transition

The low frequency Raman spectra of the γ phase (Figure 11) show an increase of the number of bands. However, the most interesting appears to be a very strong new band with the lowest frequency of 30 cm^{-1} at 7 K which shifts to 16 cm^{-1} , just below T_c , while its halfwidth increases from 1.5 to 8 cm^{-1} . This band has the characteristics of a soft mode and it has been assigned to antitranslational vibration of neighbouring chains. It has no equivalent in β phase at 50 K containing only one chain in the unit cell (Figure 9). From the behaviour of this soft mode, it can be concluded that the $\beta\leftrightarrow\gamma$ transition is of first order, of mainly displacive type and that the

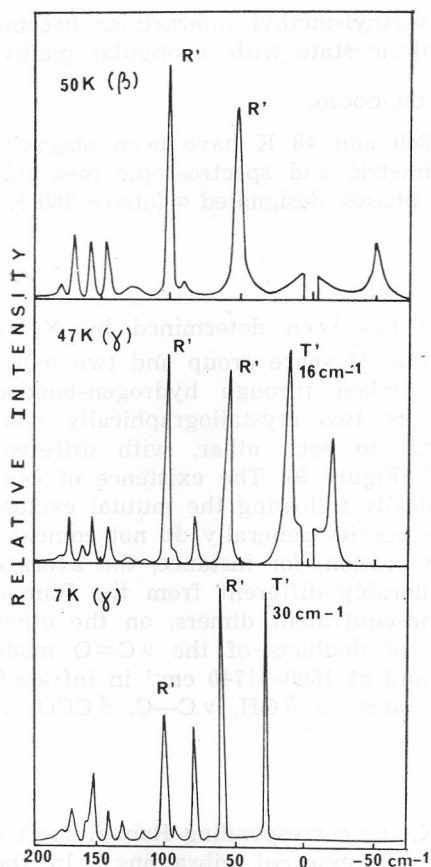


Figure 11. (left) Low-frequency Raman spectra of β and γ phase of malonic acid. After reference³⁶.

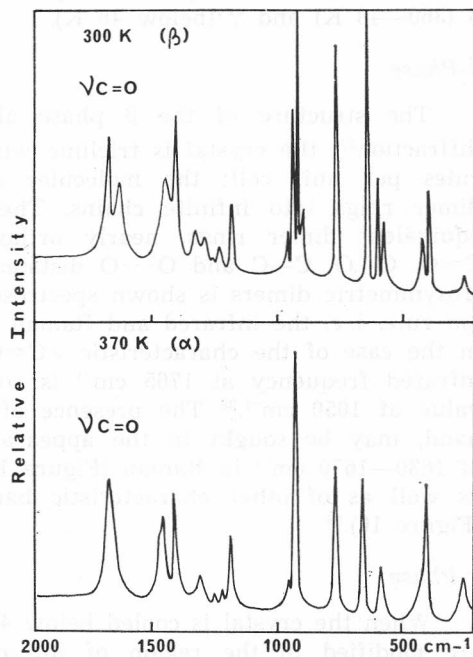


Figure 12. (right) High-frequency Raman spectra of malonic acid at 300 K (β phase) and 370 K (α phase). After reference¹⁷.

transformation mechanism must be sought in an out-of-phase gliding of infinite chains which creates new non-equivalent dimers resulting in the doubling of the unit cell.³⁶

α -Phase

When the crystal is heated above 360 K, the most significant changes are observed for carboxylic dimer bands (Figure 12). The $\nu C=O$ doublet, for instance, merges into a single band at 1665 cm^{-1} and the same happens to $\nu C-O$, δOH and γCCO doublets.¹⁷ A comparison of the infrared and Raman spectra of the α phase shows a considerable gerade-ungerade splitting for the $\nu C=O$ (1655–1730 cm^{-1}), $\delta OH + \nu C-O$ (1455–1413 cm^{-1}), δCOO (655–630 cm^{-1}) and δCCO (420–448 cm^{-1}). The molecules are thus still associated in centrosymmetric dimers forming infinite chains. The spectroscopic results of α phase, therefore, show two equivalent centrosymmetric dimer rings which implies the appearance of a glide plane the existence of which

makes ring I a mirror image of ring II (Figure 9). The space group $C2/c \equiv C_{2h}^6$ satisfies this condition: it contains four molecules in the monoclinic C-base centred cell or two molecules in the corresponding primitive cell.¹⁷

$\beta \leftrightarrow \alpha$ Transition

It has been shown that the malonic acid crystal undergoes a reversible first order phase transition at 360 K with an enthalpy change of 1.47 kJ mol⁻¹.³³ The behaviour of Raman lines for a number of modes is consistent with this conclusion since discontinuities are observed for a number of frequencies at the transition temperature. The largest discontinuities are found for carboxylic bands due to ν C=O, δ OH, ν C—O and skeletal bending motions while CH₂ scissoring frequency does not change at all.¹⁷ The most characteristic changes, however, appear in the low-frequency region (Figure 13). Two strong Raman bands due to external modes drop suddenly at T_C from 86 and 52 cm⁻¹ to 73 and 32 cm⁻¹, respectively. A detailed investigation of these bands as a function of temperature shows a hysteresis effect, as expected for a first order transition.¹⁷

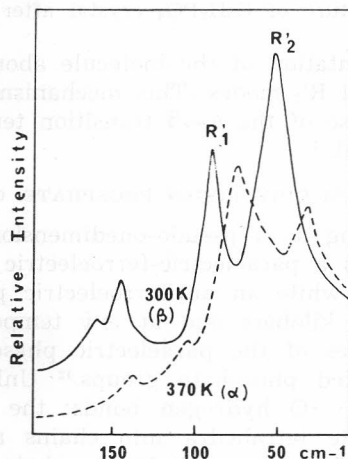


Figure 13. Low-frequency Raman spectra of malonic acid at 300 K (β phase) and 370 K (α phase). After reference¹⁷.

These two bands can be assigned to librational motions on the ground of their isotopic shifts of CD₂(COOD)₂ derivative. They consist mainly of a twisting motion of the dimer ring (γ OH...O)—R'₂ and a libration about the long molecular (dimer) axis R'₂. Softening of these two frequencies suggests that the $\alpha \leftrightarrow \beta$ structural transformation would principally result from an overall rotation of the chain of dimers about its long axis parallel to c (Figure 9). This would be accompanied by a twisting of the COOH groups, setting them along the chain with the rings roughly perpendicular to each other and associated with a shear of the whole cell along the normal to centred-base C. All these deformations have B_g symmetry in the C_{2h} group. As a result, when the molecules settle to their new equilibrium positions at the transition, the two-fold axis and the glide plane are destroyed and only the centre of symmetry is preserved. It is probable that during

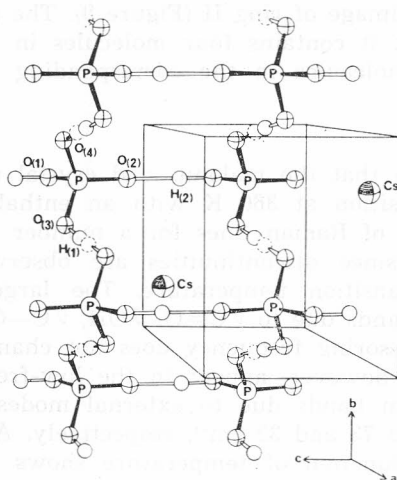


Figure 14. Structure of CsH_2PO_4 crystal after Frazer *et al.*⁴².

the transition the reorientation of the molecule about the c -axis is strongly coupled with the R'_1 and R'_2 modes. This mechanism is also consistent with a relatively small increase of the $\alpha \leftrightarrow \beta$ transition temperature of about 6 K of the $\text{CD}_2(\text{COOD})$ crystal.¹⁷

4. CESIUM DIHYDROGEN PHOSPHATE, CsH_2PO_4

CsH_2PO_4 is interesting as a pseudo-onedimensional ferroelectric crystal. Its phase diagram shows a paraelectric-ferroelectric phase transition at 153 K at normal pressure⁴⁰ while an antiferroelectric phase becomes stable at high pressure of a few kilobars and at low temperature.⁴¹

The crystal structures of the paraelectric phase (Figure 14) consist of layers of hydrogen-bonded phosphate groups.⁴² Unlike in KDP, there are two non equivalent $\text{OH} \cdots \text{O}$ hydrogen bonds: the shorter hydrogen bond (248 pm) links phosphate tetrahedra into chains along b axis while the longer hydrogen bond (254 pm) crosslinks the chains into layers. The paraelectric phase is disordered and the disorder is due to the short hydrogen bond, which can be described in terms of a statistical distribution of the proton in two off-centre equivalent sites above $T_C = 153$ K and ordered asymmetric configuration below, *i. e.* in ferroelectric phase. In this proton ordering process the crystallographic centre of inversion is lost and the $P2_1/m$ space group transforms to $P2_1$ while the number of molecules per unit cell, $Z = 2$, remains the same. The long hydrogen bond is ordered in both phases.⁴²

Paraelectric Phase

The selection rules of the C_{2h} factor group of the paraelectric phase predict 15 optically active lattice modes, $5A_g + 4B_g + 3A_u + 3B_u$, *i. e.* nine Raman and six infrared active. All these lattice bands have been observed at 234, 219, 118, 110, 75, 61, 49, 45 and 43 cm^{-1} in Raman (Figure 15) and at 220, 146, 106, 100, 76 and 38 cm^{-1} in infrared.¹⁹ The bands have been

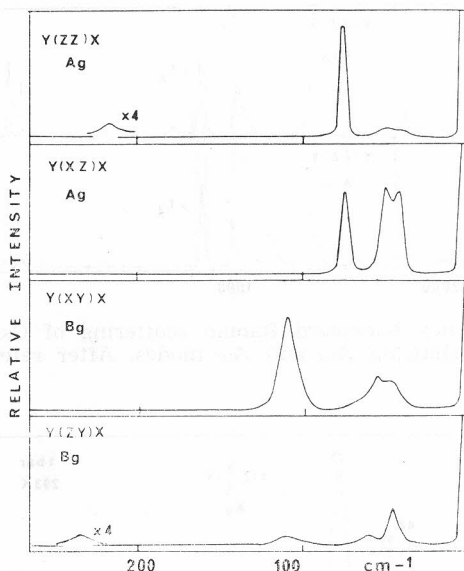


Figure 15. Low-frequency Raman spectra of CsH_2PO_4 single crystal at 300 K. After reference¹⁹.

assigned to their symmetry species using polarized radiation on single crystals, as well as to translational motions of Cs^+ cations and H_2PO_4^- anions and librations of anions employing isotopic derivatives CsD_2PO_4 and $\text{CsH}_2\text{P}^{18}\text{O}_4$ and a normal coordinate calculation.⁴³ Among these modes the Raman frequencies at 220 cm^{-1} and 75 cm^{-1} are particularly interesting: the former corresponds to a mainly short hydrogen bond stretching ($\nu\text{ OH}\cdots\text{O}$) vibration ($\text{R}'\text{b}$) and the latter to a mainly translational motion of Cs^+ ions.

The internal vibrations, on the other hand, do not obey the same selection rules and do not see centres of symmetry. It turns out that in CsH_2PO_4 , like in several other disordered crystals,^{18,21,23} the external vibrations see the (average) symmetry of the crystal in the same way as X-ray (or neutron) diffraction while the internal vibrations see only the given symmetry of a molecule or ion and not the statistical one.

Ferroelectric Phase

The symmetry lowering gives rise to new external bands in the spectra of the ferroelectric phase of CsH_2PO_4 , two infrared at 111 and 125 cm^{-1} and a Raman at 74 cm^{-1} which were forbidden in the paraelectric phase. A new kind of bands also appears in the region of both external and internal modes: this is due to the transverse optical (TO) and longitudinal optical (LO) splitting of Raman modes as a modification of selection rules of the polar ferroelectric phase. Backward scattering (180°) geometry must be used for a correct assignment of pure LO and TO components, which has been done for A modes. Significant TO—LO splitting has been observed for two external bands at 122 — 130 cm^{-1} and 205 — 249 cm^{-1} , the latter, due to short

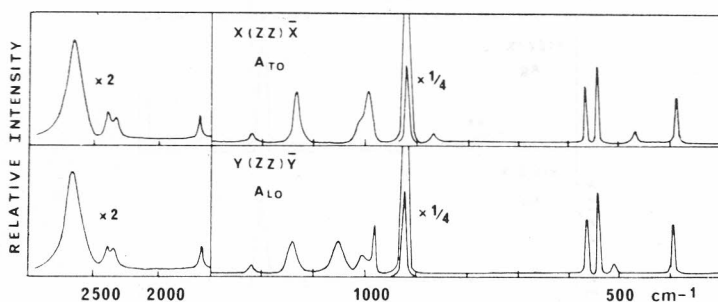


Figure 16. High-frequency backward Raman scattering of CsH_2PO_4 single crystal at 80 K showing A_{TO} and A_{LO} modes. After reference¹⁹.

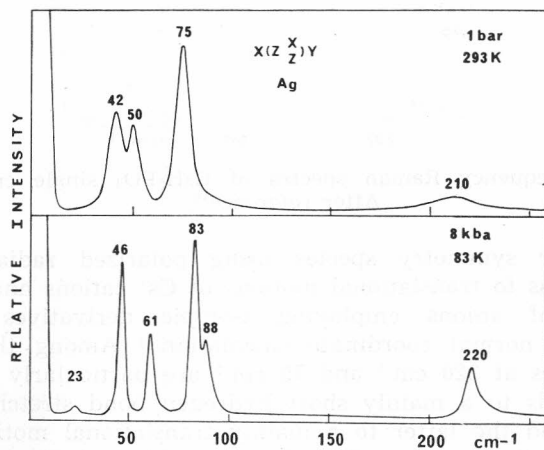


Figure 17. Low-frequency Raman spectra of CsD_2PO_4 single crystal under various pressures. After reference⁴⁴.

hydrogen bond stretching vibration, yields the highest relative splitting of about 25% and corresponds to a very strong far infrared absorption band. Several internal bands are also split and the largest splitting is found for a P—O stretching vibration at 993(TO)—1051(LO) cm^{-1} (Figure 16).¹⁹

Antiferroelectric Phase

Raman spectra of the antiferroelectric phase (AFE) of a CsD_2PO_4 single crystal were recorded at 80 K and under 8 kbar pressure.⁴⁴ Different scattering geometries showed no angular dispersion, *i. e.* no TO—LO splitting occurred to indicate that this phase was centrosymmetric. Previous neutron studies showed a doubling of the unit cell and the existence of a glide plane along \vec{a} .⁴⁵ This is confirmed by the fact that new external Raman bands at 23 and 88 cm^{-1} for A_g species (Figure 17) and 68 cm^{-1} for B_g species are observed when crossing the PE-AFE transition line. The spectroscopic results suggest the $P2_1/a$ space group with $Z = 4$ for AFE phase.⁴⁴

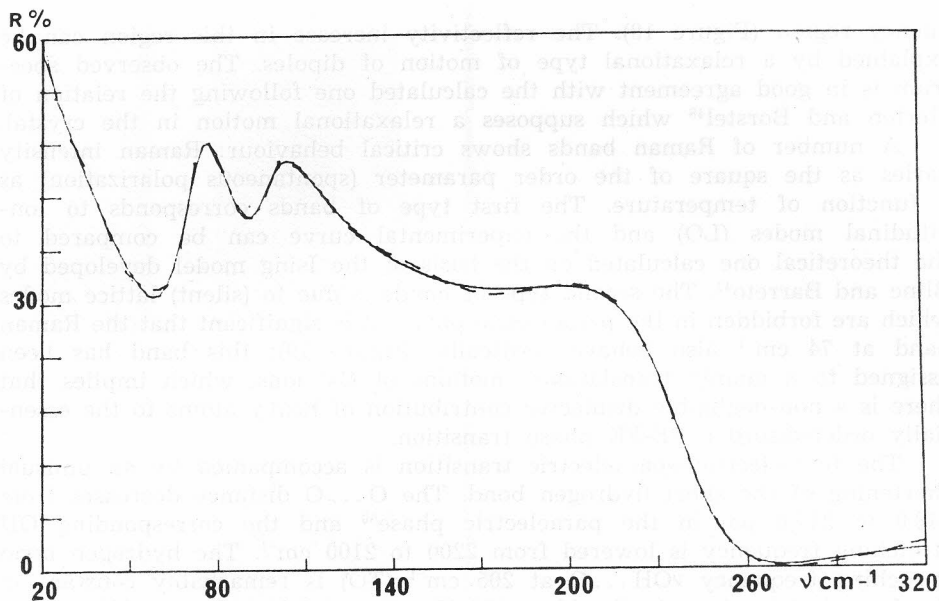


Figure 18. Infrared reflection spectrum of CsH_2PO_4 single crystal with the electric vector of the incident radiation $\vec{E} // b$ axis (A_u symmetry species) at 300 K. Full line: theoretical curve; dotted line: experimental data. After reference⁴³.

Para-ferroelectric Transition

Pseudo-one-dimensional character of CsH_2PO_4 makes the order parameter anisotropic. Zumer⁴⁶ and Blinc *et al.*⁴⁷ have shown that this anisotropy implies that the soft mode of CsH_2PO_4 has a very low frequency compared to that of KH_2PO_4 . Para-ferroelectric transition is thus expected to be governed by a relaxational rather than a resonant type of motion.

This is confirmed by the infrared reflection spectrum of a single crystal of CsH_2PO_4 which shows a wing of the central mode type in the low fre-

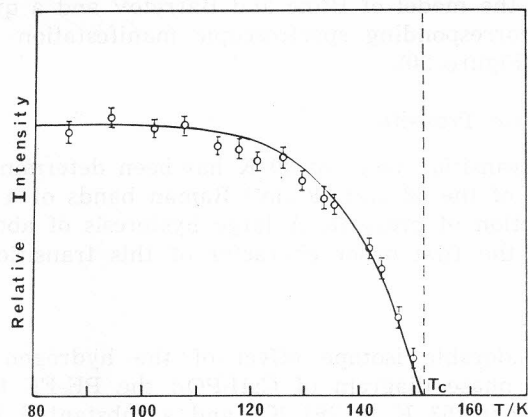


Figure 19. Intensity of the 74 cm^{-1} Raman line [$X(Y_v^X)Z$ geometry] of CsH_2PO_4 vs. temperature plot. After reference¹⁹.

quency region (Figure 18). The reflectivity increase in this region can be explained by a relaxational type of motion of dipoles. The observed spectrum is in good agreement with the calculated one following the relation of Merten and Borstel⁴⁸ which supposes a relaxational motion in the crystal.

A number of Raman bands shows critical behaviour: Raman intensity varies as the square of the order parameter (spontaneous polarization) as a function of temperature. The first type of bands corresponds to longitudinal modes (LO) and the experimental curve can be compared to the theoretical one calculated on the basis of the Ising model developed by Blinc and Barreto⁴⁷. The second type of bands is due to (silent) lattice modes which are forbidden in the paraelectric phase. It is significant that the Raman band at 74 cm^{-1} also behaves critically (Figure 19): this band has been assigned to a mainly translational motions of Cs^+ ions, which implies that there is a non-negligible displacive contribution of heavy atoms to the essentially order-disorder PE-FE phase transition.

The ferroelectric \rightarrow paraelectric transition is accompanied by an unusual shortening of the short hydrogen bond. The $\text{O}\cdots\text{O}$ distance decreases from 248.8 to 247.6 pm in the paraelectric phase⁵⁰ and the corresponding OH stretching frequency is lowered from 2200 to 2100 cm^{-1} . The hydrogen bond stretching frequency $\nu_{\text{OH}\cdots\text{O}}$ at 205 cm^{-1} (TO) is remarkably constant in the ferroelectric phase in the 80 to 153 K range and increases rapidly in the 153 to 300 K range to 220 cm^{-1} indicating that there is a continuous shortening of the $\text{O}\cdots\text{O}$ distance with temperature increase in the paraelectric phase.¹⁹

Antiferroelectric Fluctuations

A detailed investigation of single crystals of CsH_2PO_4 and CsD_2PO_4 at ordinary pressure shows that the same bands appear in the vicinity of the paraelectric-ferroelectric phase transition (Figure 20) and that their intensity reaches a maximum just at the Curie temperature. The appearance of these bands shows clearly that antiferroelectric ordering exists partially at atmospheric pressure. Such antiferroelectric fluctuations have been predicted by the model of Blinc and Barreto⁴⁷ and a quantitative interpretation of the corresponding spectroscopic manifestation was given using the above model (Figure 20).

Para-antiferroelectric Transition

The PE-AFE transition point at 80 K has been determined by measuring the intensity ratio of the 83 and 88 cm^{-1} Raman bands of a single crystal of CsD_2PO_4 as a function of pressure. A large hysteresis of about 800 bars was observed showing the first order character of this transition.⁴⁴

Isotope Effect

There is considerable isotope effect of the hydrogen substitution by deuterium on the phase diagram of CsH_2PO_4 : the PE-FE transition temperature increases from 153 K to 267 K⁴⁰ and a substantial increase of pressure is necessary to reach AFE phase.⁴¹ The deuterium also changes the $\text{O}\cdots\text{O}$ distances of both short and long hydrogen bonds. However, the short

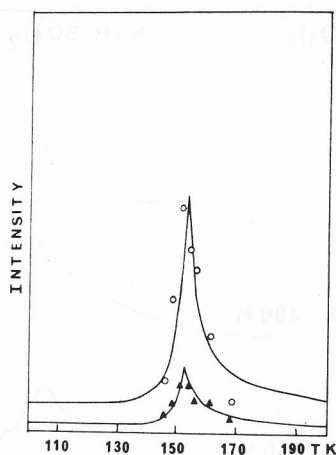


Figure 20. Intensity of the Raman lines at 25 (○) and 88 cm^{-1} (▲) of CsH_2PO_4 [X(YZ) geometry] as a function of temperature. Full lines are theoretical curves calculated following Blinc and Barreto model⁴⁷. After reference⁴⁹.

hydrogen bond expands much more, from 247.6 pm to 249.8 pm, than the long one, 253.7 to 254.0 pm.⁵⁰ This positive isotope effect is manifested spectroscopically by the lowering of the $\nu\text{OH}/\nu\text{OD}$ isotopic frequency ratio: 1.27 and 1.13 for the short and long bonds, respectively; in both cases, the ratio is much lower than 1.37, the harmonic oscillator value; another manifestation of the isotope effect is the behaviour of the $\nu\text{OH}\cdots\text{O}$ vibration of the short hydrogen bond: the temperature dependence of the half width $\Delta\nu_{1/2}$ of the corresponding $\nu\text{OH}\cdots\text{O}$ and $\nu\text{OD}\cdots\text{O}$ Raman bands is very different: the $\Delta\nu_{1/2}$ of the $\nu\text{OH}\cdots\text{O}$ band varies from 5 to 45 cm^{-1} when the temperature $T - T_C$ increases from -80 to $+140$ $^\circ\text{C}$ while there is hardly any variation of the $\Delta\nu_{1/2} = 15$ cm^{-1} of the $\nu\text{OD}\cdots\text{O}$ band under the same conditions. This difference may be related to proton jumps along hydrogen (deuterium) bonds and to different vibrational anharmonicity.

It may be argued qualitatively that the activation energy which is roughly the height of the potential barrier of the double well potential must be considerably higher for $\text{OD}\cdots\text{O}$ than for $\text{OH}\cdots\text{O}$ bond, the former being longer. The corresponding correlation time, or tunnelling probability, and halfwidth are thus expected to be smaller for $\text{OD}\cdots\text{O}$ than for $\text{OH}\cdots\text{O}$ stretching band.¹⁹

5. TRIAMMONIUM HYDROGEN DISULPHATE, $(\text{NH}_4)_3\text{H}(\text{SO}_4)_2$

At atmospheric pressure, the crystal of triammonium hydrogen disulphate (NHS) undergoes five phase transitions⁵¹⁻⁵³ and the six corresponding phases are represented as follows:

	78	133	137	265	413	
VII	V	IV	III	II	I	T/K

The room temperature phase II belongs to the monoclinic system with $A2/a$ space group and two formula entities in the unit cell. The NH_4^+ ions

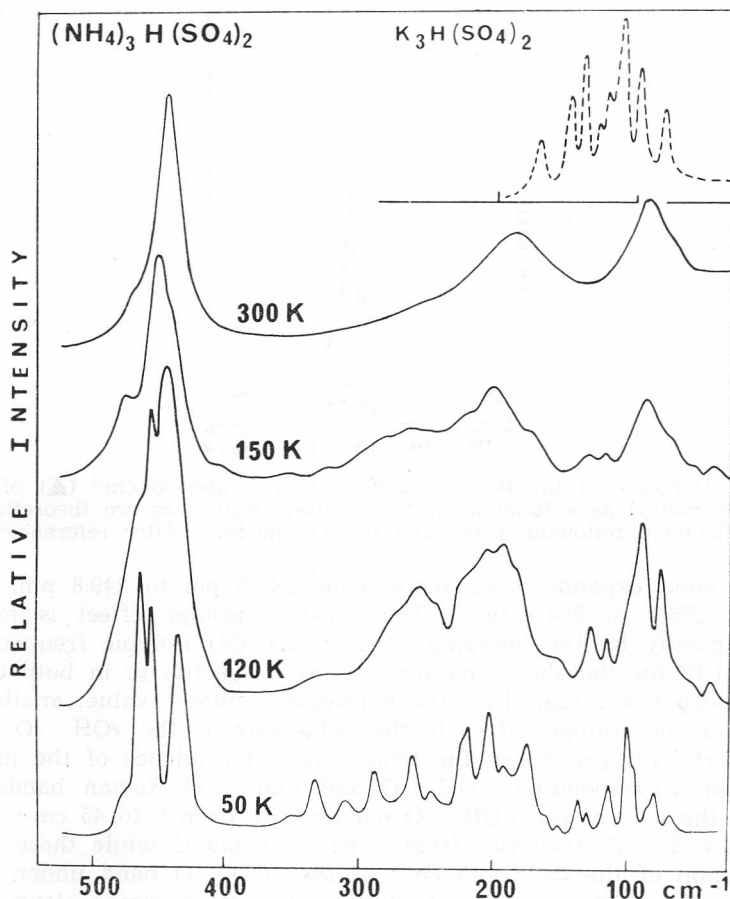


Figure 21. Low-frequency Raman spectra of $(\text{NH}_4)_3\text{H}(\text{SO}_4)_2$ at 300 K (phase II), 150 K (phase III), 120 K (phase V) and 50 K (phase VII). Dotted line: Raman spectrum of isomorphous $\text{K}_3\text{H}(\text{SO}_4)_2$ recorded for comparison. After reference²¹.

form complex $\text{NH}\cdots\text{O}$ hydrogen bonds and occupy two sites of non-equivalent positions, one of which is presumed ordered. The SO_4^{2-} ions form centrosymmetric one proton dimers via strong $\text{OH}\cdots\text{O}$ hydrogen bonds 254 pm long.⁵⁴ Phase III also appears to be monoclinic with $P2/b$ space group⁵⁵ while phase VII is ferroelectric and thus non-centrosymmetric.^{53,4}

Raman and infrared spectra of each of the investigated phases II, III, V and VII are different and allow characterizing the given phase unambiguously (Figures 21 and 22). The largest spectral differences are observed in the low frequency region below 500 cm^{-1} (Figure 21) and in the high frequency NH stretching region (Figure 22). The bands of the room temperature phase, particularly the low frequency bands due to external vibrations, are quite broad indicating that phase II is strongly disordered. In fact, there are two kinds of disorder in NHS crystal: the first is due to a statistical or dynamical distribution of proton in a crystallographically centrosymmetric hydrogen bond⁵⁴ similar to that in paraelectric phase of CsH_2PO_4 ⁴² and the second to an orien-

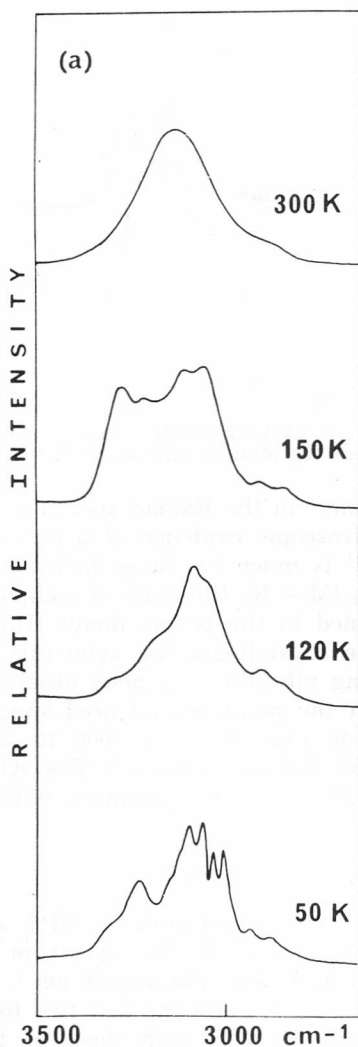


Figure 22. Raman spectra of $(\text{NH}_4)_3\text{H}(\text{SO}_4)_2$ in NH stretching region at 300 K (phase II), 150 K (phase III), 120 K (phase V) and 50 K (phase VII). After reference²¹.

tational disorder of ammonium ions. A relative ordering is observed when the temperature is lowered and ammonium ions appear to be involved in all phase transitions. Only the polar phase VII presents narrow bands or fine structure and its Raman spectrum is characteristic of a fully ordered molecular crystal.

Room Temperature Phase II

If the $(\text{SO}_4\text{HSO}_4)^{3-}$ dimers are truly centrosymmetric, the OH group vibrations are forbidden in Raman and only one totally symmetric stretching $\nu_1\text{SO}_4$ mode (Ag) is expected for a dimer. The fact that two strong Ag bands

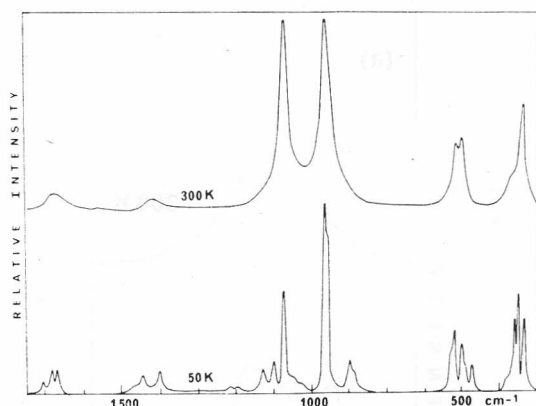


Figure 23. Raman spectra of $(\text{NH}_4)_3\text{H}(\text{SO}_4)_2$ single crystal at 300 K (phase II, ZZ scattering geometry showing A_g modes) and at 50 K (phase VII). After reference²¹.

appear at 966 and 1078 cm^{-1} in the Raman spectrum of NHS (Figure 23) may be considered as a spectroscopic evidence of a non centrosymmetric dimer.⁵⁶ The splitting of 112 cm^{-1} is much too large to be due to a correlation field. By analogy with MHSO_4 ($M = \text{K}, \text{Na}$) type of compounds,⁵⁷ the 966 and 1070 cm^{-1} bands can be assigned to the proton donor (HSO_4^-) and acceptor (SO_4^{2-}) groups, respectively. The crystallographic symmetry is thus of a statistical nature. The OH stretching vibration has been observed as a very strong and broad absorption (Au) in the polarized infrared spectrum of a single crystal of NHS.⁵⁵ This absorption extends from 2000 to 300 cm^{-1} , with characteristic Evans holes at 1030, 888 and 446 cm^{-1} . The νOH centre of gravity frequency is found near 1200 cm^{-1} , in agreement with the $\text{O}\cdots\text{O}$ distance of 254 pm.

Low Temperature Phases III, V and VII

The low frequency Raman spectrum of NHS appears to be the most temperature sensitive (Figure 21). In the spectrum of phase II only three broad bands are observed near 440, 185 and 80 cm^{-1} ; the first has been assigned to the $\nu_2\text{SO}_4^{2-}$ bending modes and the last two to the external vibrations. Comparison of the spectra of NHS with those of the isomorphous crystal, $\text{K}_3\text{H}(\text{SO}_4)_2$ (KHS) at various temperatures, shows that the latter exhibits narrow bands already at room temperature while the former are changed gradually and become narrow and structured only in phase VII below 78 K. This indicates that the $\text{OH}\cdots\text{O}$ hydrogen bond disorder in dimers does not affect much the band breadth in KHS and thus neither in NHS. The main responsible factor of the band broadening is thus the disorder of ammonium ions which must be responsible for phase transitions. No phase transition has been reported for KHS.

In phase III, there is some structure in the low frequency (Figure 21) and NH stretching region (Figure 22) but on the whole the spectral pattern is similar to that of phase II. The $\text{II} \leftrightarrow \text{III}$ transition involves a unit cell doubling and a rearrangement of $\text{NH}\cdots\text{O}$ hydrogen bonds but not a significant ordering of ammonium ions. The spectral data are consistent with the $P2/b$ space group and $Z = 4$ given by X-ray diffraction.⁵⁵ This space group implies

the disappearance of one of the two centres of inversion: the $(\text{SO}_4\text{HSO}_4)^{3-}$ dimers may, therefore, be on general positions and the $\text{OH}\cdots\text{O}$ hydrogen bonds become ordered but remain asymmetric. However, this does not change much the splitting of the $\nu_1\text{SO}_4$ bands; the dimer structure and its $\text{O}\cdots\text{O}$ length are believed to be very similar to those of phase II.²¹

Phase V at 120 K is characterized by a strong enhancement of the NH stretching absorption and by considerable narrowing of lattice bands. New bands assigned to NH_4^+ librations appear in the 300 to 230 cm^{-1} region, showing that a serious ordering of ammonium ions occurs.

Finally, phase VII at 50 K appears fully ordered at least as far as NH_4^+ ions are concerned. The low frequency Raman spectra consist of numerous narrow bands and the distinction between NH_4^+ and HSO_4^- librations becomes possible. The $V \leftrightarrow VII$ phase transitions are a first order transition since there are discontinuities in the Raman frequency *versus* temperature plot. It is of order-disorder type and the main mechanism appears to be the orientational ordering of ammonium ions. The latter contributes mostly to the ferroelectricity of phase VII, in any case much more than the ordering of protons in sulphate dimers.²¹

6. CESIUM HYDROGEN SULPHATE, CsHSO_4

Cesium hydrogen sulphate aroused a considerable interest since its high temperature phase above 417 K exhibits unusually high conductivity⁵⁸ of the order of $10^{-2} \Omega^{-1} \text{cm}^{-1}$. It belongs, thus, to superionic protonic conductors and these materials may be used potentially in various conversion systems such as fuel cells, capacitors, sensors or electrochromic displays.⁵⁹

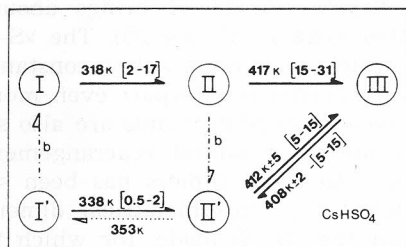


Figure 24. Diagrammatic representation of temperature and enthalpy changes of phase transitions in CsHSO_4 . After reference²³.

Calorimetric and spectroscopic measurements^{23,60} show that the phase transformations of CsHSO_4 depend considerably on the thermal history of the sample and on pressure. On heating a freshly prepared crystal the room temperature phase I goes to phase II at 318 K and to phase III at 417 K while on cooling phase II' at 408 K and phase I' at 353 K were obtained instead of phases II and I (Figure 24). The infrared and Raman spectra of all these phases are different.

Phase I

Crystalline structure of CsHSO_4 at room temperature has been determined by X-ray diffraction.⁶¹ The monoclinic crystal belongs to $P2_1/m$ (C^{2h}) space group with two formula units per unit cell. There are infinite hydrogen

bonded chains of SO_4 tetrahedra with the $\text{O}\cdots\text{O}$ distance of 257.2 pm and the proton appears to be disordered between two equilibrium sites creating a statistically symmetric hydrogen bond. On the whole, the structure of CsHSO_4 is very similar to that of the paraelectric phase of CsH_2PO_4 apart for the extra hydrogen (long hydrogen bond) in the latter (Figure 14). There is also a similarity with the structure of ionic conductors such as Li_2SO_4 , LiNaSO_4 or even NASICON.^{62,63}

Vibrational spectra are consistent with the X-ray diffraction results. The selection rules derived from the C_{2h} symmetry are obeyed by external vibrations: the single crystal Raman spectra show 3Ag and 4Bg bands out of 5Ag + 4Bg predicted and polarized infrared reflection spectra 3Au and 1Bu out of 3Au + 3Bu. The low frequency bands at 40, 50 and 60 cm^{-1} have been assigned to mainly Cs^+ translational and the high frequency bands at 215, 190 and 115 cm^{-1} to mainly librational motions of HSO_4^- ions by analogy with the spectra of CsH_2PO_4 .¹⁹ Internal vibrations, on the other hand, see neither centres nor planes of symmetry and, in particular, the Raman bands due to $\nu\text{S}(\text{OH})$ (donor) and $\nu\text{S}(\text{O})$ (acceptor) vibrations identified at 865 and 995 cm^{-1} , respectively, show that each given $\text{OH}\cdots\text{O}$ hydrogen bond is asymmetrical and that the crystallographic symmetry is statistical.

The structure of phase I appears to be the same down to liquid helium temperature and no spectroscopic evidence of a ferroelectric ordered phase, a possibility suggested by Itoh *et al.*⁶¹, has been found.

Phase II

Heating of CsHSO_4 crystal to 350 K brings about significant changes both in internal and lattice regions (Figure 25). The $\nu\text{S}(\text{O})$ (acceptor) Raman frequency at 998 cm^{-1} which was remarkably constant from 18 to 300 K rises to 1024 cm^{-1} and its infrared counterpart even more, from 1000 to 1050 cm^{-1} and broadens. The skeletal bending bands are also significantly modified. These changes reflect a more substantial rearrangement of SO_4 tetrahedra and a conversion of chains to cyclic dimers has been suggested.⁶⁴ A mutual exclusion rule is expected for centrosymmetrical dimers and this has been observed, in particular for the $\nu\text{S}(\text{O})$ mode, for which the largest ungerade-gerade splitting 1050—1024 cm^{-1} has been found. This conversion of chains into dimers is accompanied by a weakening of the hydrogen bond: the difference between the $\nu\text{S}(\text{O})$ and $\nu\text{S}(\text{OH})$ frequencies increases and the OH stretching band shifts by about 100 cm^{-1} towards higher wave-numbers. It should be pointed out that on some other alkali hydrogen sulphates HSO_4^- anions pass easily from chains to ring dimers, α and β phases of NaHSO_4 ,⁶⁵ for instance, contain chains and dimers, respectively while in KHSO_4 crystal both forms coexist.⁶⁶

In the low frequency region the Raman bands due to mainly librational motions of HSO_4^- anions disappear or broaden while those corresponding to mainly translational modes of Cs^+ cations are less affected.

On the whole, the spectral data show that the $I \leftrightarrow II$ transition is of first order (discontinuity in the S—O stretching frequency *versus* temperature plot) and of reconstructive type with a structural transformation of infinite chains into ring dimers, an increased orientational disorder of anions and weakening of $\text{OH}\cdots\text{O}$ hydrogen bonds.

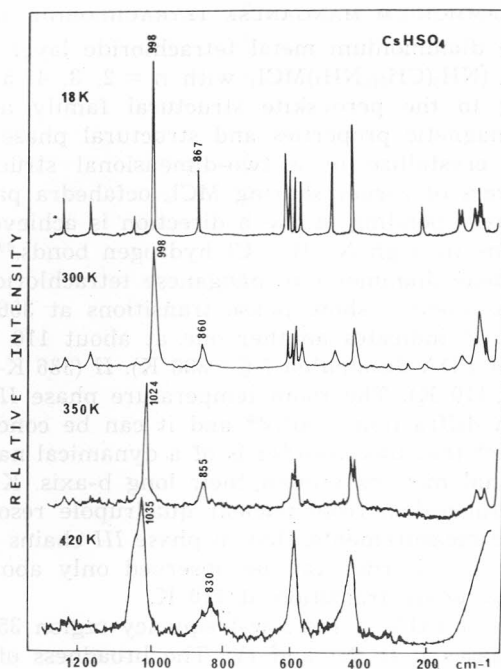


Figure 25. Raman spectra of polycrystalline CsHSO_4 at 18 and 300 K (phase I), 350 K (phase II) and 420 K (phase III). After reference⁶⁴.

Phase III

The spectroscopic changes of phase III (Figure 25) consist of broadening of the skeletal stretching and bending Raman bands and further diminishing of their number. This indicates a higher (average) symmetry of this phase and certainly a highly disordered structure. The most dramatic changes, however, are observed for external modes where all the bands collapse into a broad wing near the Rayleigh line.

This behaviour is characteristic of a plastic phase of molecular crystals and implies a »free« rotation of HSO_4^- ions on given sites. Moreover, the Cs^+ sublattice becomes also disordered. The Raman spectrum of phase III can thus be considered a spectroscopic manifestation of a quasi-liquid state of the superionic conductor phase. Phase III is thus both a protonic and ionic conductor while in phase II and I the conductivity is essentially protonic and this may explain the drastic increase in conductivity for almost five orders of magnitude in going from phase II to phase III.

The above conclusions agree with a recent work of Haynovskiy *et al.*⁶⁷ who found out that there is almost no difference in conductivity of phase III of CsHSO_4 and CsDSO_4 while at lower temperatures (phases II and I) the conductivity of the deuterated crystal decreases by about two orders of magnitude.

7. PROPYLENE DIAMMONIUM MANGANESE TETRACHLORIDE, $(\text{NH}_3(\text{CH}_2)_3\text{NH}_3)\text{MnCl}_4$

The propylene diammonium metal tetrachloride layer compounds having a general formula $(\text{NH}_3(\text{CH}_2)_n\text{NH}_3)\text{MCl}_4$ with $n = 2, 3, 4, 5$ and $M = \text{Cu}, \text{Mn}, \text{Fe}, \text{Cd}, \dots$ belong to the perovskite structural family and are interesting because of their magnetic properties and structural phase transitions.^{26,27,68,69} These compounds crystallize in a two-dimensional structure consisting of nearly isolated layers of corner sharing MCl_6 octahedra parallel to the (a, c) planes. The interlayer bonding in the b direction is achieved by the alkylene diammonium cations through $\text{N}-\text{H}\cdots\text{Cl}$ hydrogen bonds.^{69,70}

For the propylene diammonium manganese tetrachloride (abbr. PDA) the calorimetric measurements⁷¹ show phase transitions at 336 and 306 K while Raman spectroscopy²⁶ indicates another one at about 110 K. There are thus four solid phases of PDA designated *I* (> 336 K), *II* (336 K—306 K), *III* (306—110 K) and *IV* (< 110 K). The room temperature phase *III* is disordered according to neutron diffraction results⁶⁹ and it can be concluded from proton magnetic resonance⁶⁹ that this disorder is of a dynamical nature, the PDA ions undergoing rotational motions around their long b-axis. Kind *et al.*⁷⁰, on the other hand, have suggested, from nuclear quadrupole resonance and nuclear magnetic resonance measurements, that in phase *III* chains are almost ordered and that a dynamical disorder can be observed only above 306 K. Besides, they do not see any phase transition at 110 K.

Raman spectra of PDA in the low-frequency region 350—10 cm^{-1} (Figure 26) characterize phases *I*, *II*, *III* and *IV*. The broadness of bands indicates a

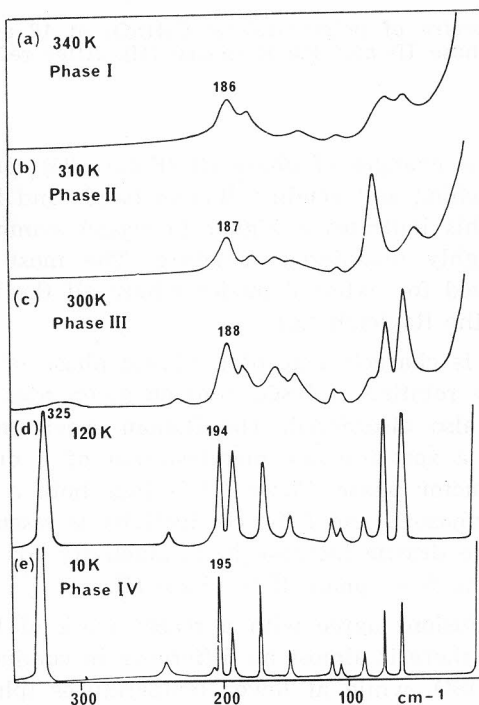


Figure 26. Low-frequency Raman spectra of $\text{NH}_3(\text{CH}_2)_3\text{NH}_3\text{MnCl}_4$ single crystal at various temperatures. After reference²⁶.

large amount of disorder in high temperature phases while only the spectrum of phase IV is that of a fully ordered crystal. Discontinuities are observed in frequency variation with temperature for $I \leftrightarrow II \leftrightarrow III$ transitions the two lowest Raman frequencies near 60 and 70 cm^{-1} assigned to chlorine atom motions being the most sensitive. The above results confirm the first order character of the $I \leftrightarrow II \leftrightarrow III$ transitions.^{70,71} The frequency and half-width variation of Raman bands of PDA are continuous between 10 and 300 K but the corresponding curves present an inflection point at about 110 K. The infrared spectra of four different phases are also different, in particular in the NH_3 bending (1620—1400 cm^{-1}) and MnCl stretching (480—200 cm^{-1}) regions.²⁶

There is some controversy about the structure of phase III. A neutron diffraction study⁶⁹ gives $Imma \equiv D_{2h}^{28}$ space group with $Z = 2$ while NQR dielectric and optical results appear to be consistent with $Pnma \equiv D_{2h}^{16}$ symmetry and $Z = 4$. Raman and infrared spectra of single crystals of PDA agree better with the structure proposed by neutron diffraction⁶⁹ on the ground of the number of observed external bands.²⁶ The spectra of phase IV can also be interpreted in terms of D_{2h} factor group with $Z = 2$.

As far as the $III \leftrightarrow IV$ phase transition is concerned, the most sensitive Raman bands are those assigned to the torsion of NH_3^+ group at 325 cm^{-1} , stretching $\text{Mn}-\text{Cl}$ vibrations near 320 and 200 cm^{-1} and the libration of the cation $^+\text{NH}_3(\text{CH}_2)_2\text{NH}_3^+$ around its long axis ($R'y$) near 190 cm^{-1} . The curves in the frequency *versus* temperature plot present an inflection point at about 100 K. From the variation of the torsional NH_3 frequency, the thermal expansion coefficient could be determined, $\gamma = -0.25 \times 10^{-3}$ and $-0.40 \times 10^{-3} \text{ K}^{-1}$ below 120 and above 150 K, respectively. The most dramatic change, however, is observed for the integrated intensity of NH_3 torsional band (Figure 26). This is the strongest Raman band in phase IV at 10 K but its intensity decreases very rapidly above 100 K and the band is hardly observed in the room temperature phase. It also presents an inflection point at 110 K. The corresponding curve $I = f(T)$ reflects a thermally activated process governed by Boltzmann's law: when the temperature is raised, an increasing proportion of NH_3 groups start to jump and escape to the Raman observation while the Rayleigh line broadens. Finally, from the half-width variation of the τNH_3

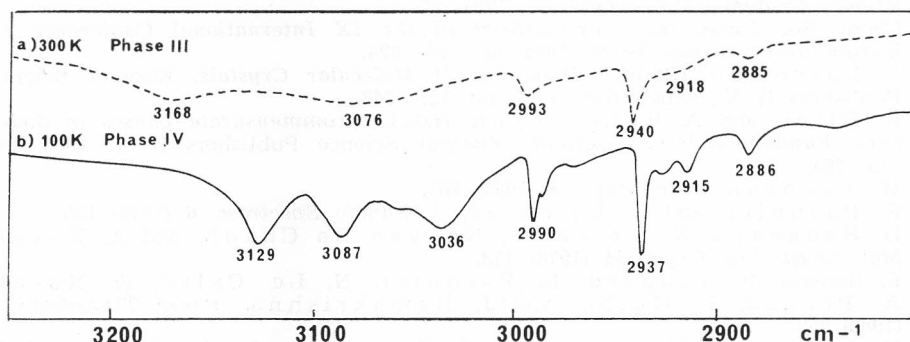


Figure 27. Infrared spectra (NH stretching region) of an isotopically diluted crystal of $\text{ND}_3(\text{CH}_2)_3\text{ND}_3\text{MnCl}$ containing about 5% of hydrogenated compound at 300 and 100 K. After reference²⁶.

band with temperature it can be concluded that the life-time of the torsional mode is limited, at high temperature, mainly by the rotational jumps of NH_3^+ groups. The experimental curve for NH_3 torsion has been fitted to the equation⁷² $\Gamma_{1/2} = (a + bT) + (c' \nu_0 \exp - E_0/kT)$ where $\Gamma_{1/2}$ is the half width of the phonon, a , b and c' constants and E_0 the activation energy corresponding approximately to the potential barrier V_0 governing the disorder mechanism. The obtained value $E_0 = 4.2 \text{ kJ mol}^{-1}$ can be compared with the six-fold potential barrier, derived from the torsional frequency, $V_0 = 5.0 \text{ kJ mol}^{-1}$. The correlation time $\tau_c = \tau_0 \exp E_0/kT$ is then $1.5 \times 10^{-11} \text{ s}$ at 100 K and $5.6 \times 10^{-13} \text{ s}$ at 300 K. At room temperature the correlation time is of the same order of magnitude as the observation time and this could explain the fact that at 300 K the infrared spectrum of an isotopically diluted sample of PDA shows only a broad diffuse absorption in the NH stretching region (Figure 27). At 100 K, on the other hand, the residence time would be long enough to distinguish three non-equivalent protons, *i.e.* three NH stretching bands at 3120, 3087 and 3036 cm^{-1} (Figure 27). The broadening of the R'y librational band of PDA cation can be partly explained by the same type of process: above 250 K it seems that a certain proportion of cations is already jumping; both NH_3 torsion and R'y libration can get coupled and induce the next $III \leftrightarrow II$ transition.

A recent neutron scattering study²⁷ of PDA confirms that the reorientational motions of protons of NH groups take place in phases III and IV . However, the dynamics of NH_3 groups at room temperature is governed by a correlation time $\tau = 1 \times 10^{-11} \text{ s}$ and by an activation energy of 26.6 kJ mol^{-1} . The value of 4.24 J mol^{-1} observed from Raman line broadening is thus considerably underestimated.

REFERENCES

1. J. F. Scott, *Rev. Modern Physics* **46** (1974) 83.
2. J. Petzelt and V. Dvorak, *J. Phys. C* **9** (1976) 1571.
3. P. A. Fleury, *J. Acoust. Soc. Am.* **49** (1971) 1041.
4. E. V. Chopler in: M. M. Sushchinski (Ed.), *Sovremennyye problemy spektroskopii kombinacionnogo rasseyaniya sveta*, Moscow, Nauka 1978, pp. 70—91.
5. J. Lascombe and P. V. Huong, (Eds.), *Raman Spectroscopy. Linear and Non-linear*, J. Wiley and Sons, New York 1982, pp. 387—526.
- 5a. Z. Iqbal and F. J. Owens, Eds., *Vibrational Spectroscopy of Phase Transitions*, Academic Press, Orlando, 1984.
6. Chem. Soc Japan (Ed.), *Proceedings of the IX International Conference on Raman Spectroscopy*, Tokyo 1984, pp. 796—824.
7. J. Lascombe (Editor), *Dynamics of Molecular Crystals*, Elsevier Science Publishers B. V., Amsterdam 1987, pp. 121—243.
8. R. Blinc and A. P. Levanyuk (Eds.), *Incommensurate phases in dielectrics. Fundamentals*, Amsterdam, Elsevier Science Publishers B. V. 1986, pp. 315—364.
9. W. Cochran, *Adv. Phys.* **9** (1960) 387.
10. B. Pasquier and N. Le Calvé, *J. Raman Spectrosc.* **6** (1977) 155.
11. D. Bougeard, N. Le Calvé, Nguyen Ba Chanh, and A. Novak, *Mol. Cryst. Liq. Cryst.* **44** (1978) 113.
12. F. Romain, P. Tougaard, B. Pasquier, N. Le Calvé, A. Novak, A. Péneau, L. Guibé, and J. Ramakrishna, *Phase Transitions* **3** (1983) 259.
13. N. Le Calvé, B. Pasquier, G. Braathen, L. Soulard, and F. Fillaux, *J. Phys. C: Solid State Phys.* **19** (1986) 6695.
14. N. Le Calvé, B. Pasquier, and A. Novak, *J. Chem. Phys.* **72** (1980) 6409.

15. M. Krauzmann, R. M. Pick, N. Le Calvé, and B. Pasquier, *J. Physique* **44** (1983) 849.
16. J. de Villepin, D. Bougeard, and A. Novak, *Chem. Phys.* **73** (1982) 291.
17. J. de Villepin, M. H. Limage, A. Novak, N. Toupry, M. Le Postollec, H. Poulet, S. Ganguly, and C. N. R. Rao, *J. Raman Spectrosc.* **15** (1984) 41.
18. D. Bougeard and A. Novak, *Solid State Commun.* **27** (1978) 453.
19. B. Marchon and A. Novak, *J. Chem. Phys.* **78** (1983) 2105.
20. B. Marchon, A. Novak, and R. Blinc, *J. Raman Spectrosc.* (1987).
21. M. Kamoun, A. Lautié, F. Romain, A. Daoud, and A. Novak, in J. Lascombe (Editor), *Dynamics of Molecular Crystals*, Amsterdam, Elsevier Science Publishers B. V., 1987, p. 219.
22. M. Pham Thi, Ph. Colomban, and A. Novak, *J. Phys. Chem. Solids* **46** (1985) 565.
23. M. Pham Thi, Ph. Colomban, A. Novak, and R. Blinc, *Solid State Commun.* **55** (1985) 265.
24. Ph. Colomban, M. Pham Thi, and A. Novak, *J. Mol. Struct.* (1987).
25. J. Kress and A. Novak, *J. Mol. Struct.* **23** (1974) 215.
26. C. Sourisseau and G. Lucazeau, *J. Raman Spectrosc.* **8** (1979) 311.
27. C. Sourisseau, G. Lucazeau, and A. J. Dianoux, *J. Physique* **44** (1983) 967.
28. K. Chhor, C. Sourisseau, and G. Lucazeau, *J. Raman Spectrosc.* **11** (1981) 183.
29. A. Péneau, M. Gourdji, and L. Guibé, *J. Mol. Struct.* **111** (1983) 227.
30. O. Ohms, H. Guth, W. Treutmann, H. Dannöhl, A. Schwerig, and G. Heger, *J. Chem. Phys.* **83** (1985) 273.
31. S. G. Biswas, *Ind. J. Phys.* **35** (1968) 261.
32. B. Alefeld, A. Kollmar, and B. Dassanacharya, *J. Chem. Phys.* **63** (1975) 4415.
33. S. Ganguly, J. R. Fernandez, G. R. Desiraju, and C. N. R. Rao, *Chem. Phys. Lett.* **69** (1980) 227.
34. H. Suga, personal communication.
35. C. N. R. Rao, S. Ganguly, and H. R. Swamy, *Croat. Chem. Acta* **55** (1982) 207.
36. C. Pigenet, G. Lucazeau, and A. Novak, in *Molecular Spectroscopy of Dense Phase*, edited by M. Grossmann et al., Elsevier, Amsterdam (1976) p. 311.
37. J. A. Goedkoop and C. H. MacGillavry, *Acta Crystallogr.* **10** (1957) 125.
38. C. Pigenet, G. Lucazeau, and A. Novak, *J. Chim. Phys.* **73** (1976) 141.
39. W. Derbyshire, T. C. Gorvin, and D. Wormer, *Mol. Phys.* **17** (1969) 401.
40. A. Levstik, R. Blinc, P. Kabada, S. Cizikov, I. Levstik, and C. Filipic, *Solid State Comm.* **16** (1975) 1339.
41. N. Yasuda, M. Okamoto, H. Shimizu, S. Fujimoto, K. Yoshino, and Y. Inuishi, *Phys. Rev. Lett.* **41** (1978) 1311.
42. B. C. Frazer, D. Semmingsen, W. D. Ellenson, and G. Shirane, *Phys. Rev.* **B20** (1979) 2745.
43. B. Marchon, *Thesis*, Paris (1983).
44. B. Marchon, M. Krauzmann, and A. Novak, *J. Mol. Struct.* **79** (1982) 381.
45. R. Youngblood, B. B. Frazer, J. Eckert, and G. Shirane, *Phys. Rev.* **B22** (1980) 228.
46. S. Zumer, *Ferroelectrics* **25** (1980) 419.
47. R. Blinc and F. C. Sa Barreto, *J. Chem. Phys.* **72** (1980) 6031.
48. L. Merten and G. Borstel, *Phys. Status Solid* **B77** (1976) 221.
49. B. Marchon and A. Novak, *Ferroelectrics* **55** (1984) 728.
50. D. Semmingsen and R. Thomas, unpublished results.
51. K. Gesi, *Phys. Status Solidi* **A33** (1976) 479.
52. S. Suzuki, Y. Oshino, K. Gesi, and Y. Makita, *J. Phys. Soc. Japan* **47** (1979) 874.
53. K. Gesi, *Japan J. Appl. Phys.* **19** (1980) 1051.

54. S. Suzuki and Y. Makita, *Acta Cryst.* **B34** (1978) 732.
55. M. Kamoun, *Thesis*, Sfax, Tunisia (1987).
56. M. Damak, M. Kamoun, A. Daoud, F. Romain, A. Lautié, and A. Novak, *J. Mol. Struct.* **130** (1985) 245.
57. A. Goypiro, J. de Villepin, and A. Novak, *J. Raman Spectrosc.* **9** (1980) 297.
58. A. T. Baranov, L. A. Shuvalov, and N. M. Shchagina, *J. E. P. T. Lett.* **36** (1982) 459.
59. J. B. Goodenough, J. Jensen, and A. Potier eds., *Solid State Protonic Conductors III for Fuel Cells and Sensors*, Odense University Press (1985).
60. Ph. Colombar, M. Pham-Thi, and A. Novak, *Solid State Ionics* **20** (1986) 125.
61. F. Itoh, T. Ozaki, and E. Nakamura, *Acta Cryst.* **B37** (1981) 1908.
62. H. Schulz, V. Zucker, and G. Frech, *Acta Cryst.* **B41** (1985) 21.
63. H. Y. P. Hong, *Mat. Res. Bull.* **11** (1976) 173.
64. M. Pham Thi, Ph. Colombar, A. Novak, and R. Blinc, *J. Raman Spectrosc.* **18** (1987).
65. F. J. Sonneveld and J. W. Visser, *Acta Cryst.* **B35** (1979) 1975
66. F. A. Cotton, B. A. Frenz, and D. L. Hunter, *Acta Cryst.* **B31** (1975) 302.
67. N. G. Hainovskiy, Yu. T. Pavlyuhin, and E. F. Huyretdinov *Izv. Sibir. Otd. ANSSSR, Ser. Khim. Nauk.* **11** (1985) 99.
68. R. Blinc, M. Burgar, M. Lozar, J. Seliger, J. Slak, V. Pucar, H. Arend, and R. Kind, *J. Chem. Phys.* **66** (1977) 278.
69. R. D. Willett and E. R. Riedel, *Chem. Phys.* **8** (1975) 112.
70. R. Kind, S. Plesko, and J. Roos, *Phys. Status Solid* **A47** (1978) 233.
71. H. Arend, K. Tichy, K. Baberschke, and F. Rys, *Solid State Commun.* **18** (1976) 999.
72. P. da R. Andrade, A. D. Prasad Rao, R. S. Katiyor, and S. P. S. Porto, *Solid State Commun.* **12** (1973) 847.

IZVLEČEK

A. Novak

Vibracijska spektroskopija in strukturni fazni prehodi molekulskih kristalov

Vibracijska spektroskopija lahko preskrbi koristne strukturne in dinamične podatke o faznih prehodnih v molekulskih kristalih, posebno tiste o mehanizmu strukturne transformacije na molekulski ravni. Pričujoči članek pokaže to s primeri različnih tipov kristalov — od čisto vanderwaalsovskih (3,5-diklorpiridin in 4-metilpiridin) preko vodikovo vezanih organskih kristalov (malonska kislina) in anorganskih feroelektrikov (CsH_2PO_4 in $(\text{NH}_4)_3\text{H}(\text{SO}_4)_2$) do superionskega protonskega prevodnika CsHSO_4 in koordinacijske spojine $(\text{NH}_3(\text{CH}_2)_3\text{NH}_3)\text{MnCl}_4$.